Asociación Argentina
de Mecánica Computacional

Mecánica Computacional Vol XXXI, págs. 723-733 (artículo completo)
Alberto Cardona, Paul H. Kohan, Ricardo D. Quinteros, Mario A. Storti (Eds.)
Salta, Argentina, 13-16 Noviembre 2012

# FINITE ELEMENT SIMULATION OF BIOLOGICAL VISCOUS MEMBRANES

**Roberto F. Ausas, Diego S. Rodrigues and Gustavo C. Buscaglia**

*Instituto de Ciências Matemáticas e de Computação, Universidade de São Paulo, Av. do Trabalhador são-carlense 400, 13560-970 São Carlos, SP, Brazil, rfausas@gmail.com*

**Keywords:** Biological Membranes, Lipidic Bilayer, Willmore Flow, Finite Elements.

**Abstract.** In this work we study the dynamical behavior of biological membranes subject to area and volume constraints. The membrane is discretized by a surface mesh made of linear or quadratic triangular elements whose nodes are explicitly updated at each time step. The Stokes operator on the surface is solved using linear or quadratic elements for velocity and membrane pressure with stabilization by pressure gradient projection. The volume constraint is treated by adding an internal pressure. The membrane curvature is computed either by using Meyer's method or the Laplace-Beltrami identity and both methods compared. The different ingredients present in our formulation are detailed throughout the work and presented together with examples in three spatial dimensions.

## 1 INTRODUCTION

Biological membranes, such as lipossomes, consist of lipid bilayers that rheologically behave as two-dimensional viscous fluids embedded in three dimensional space. This model is reasonable because of the large difference between their thickness (a few nanometers) and their macroscopic size ($\sim$ 100 micrometers). Typical surface viscosities range from $10^{-9}$ to $10^{-6}$ $Pa\text{-}s\text{-}m$ (Seifert (1999); Waugh (1982)). Modeling of such systems is a challenging task, both mathematically and numerically, since it requires solving the viscous operator on a time evolving curved surface governed by an elastic energy that depends on its mean curvature and which is also subjected to inextensibility (area) and volume constraints. The area constraint is not just global, but it is a local one, since the number of lipid molecules is known to be related to the local surface area of the membrane. The volume constraint comes from the fact that the membranes are sourrounded by incompressible fluids. Eventually, some osmotic activity can be present in the membrane which would induce a flow across the membrane.

Different solution techniques are already available in the literature to solve such problems (see for instance Bänsch et al. (2005); Bonito et al. (2010); Barrett et al. (2008)), but most of them concentrate on the resolution of geometric or gradient flows originated by the elastic energy and considering the volume and/or area constraints. In some cases, the interaction with the sourrounding bulk fluids is also considered (see Salac and Miksis (2011); Bonito et al. (2011)), but surface viscous effects were in general ignored. Their importance have started to be recognized recently in Arroyo and DeSimone (2009) in which the relaxation of biological membranes is thoroughly studied numerically with a 3D axially symmetrical model. Full three dimensional simulations of problems involving surface viscous effects are more difficult to find (see e.g. Buscaglia and Tasso (2011)). Surface viscous effects are accounted by solving the Stokes operator on the membrane according to the Boussinesq-Scriven law, which is basically the analogue of the usual Newtonian constitutive law. Although in a different framework, this is done for instance in Pozrikidis (1994); Gross and Reusken (2011); Bothe and Prüss (2010). Viscoelastic effects are supossed to be unimportant.

In this work we present a three dimensional finite element methodology with explicit representation of the interface to study the behavior of membranes focusing on surface viscous effects. In order to impose the inextensibility constraint to some extent, a possibility explored here, consists in increasing one of the surface viscosity coefficients with respect to the other in the Boussinesq-Scriven law mentioned above. The other possible approach is including a variable surface tension coefficient or membrane pressure, acting as a local Lagrange multiplier for the restriction. The two options are compared later on. On the other hand, the volume constraint is accounted for by means of an internal pressure acting as a global Lagrange multiplier. Also, different ways to computing the curvature, which is a key issue in these problems, are tested.

After this introduction, the mathematical formulation of the problem is presented in a variational framework well suited for discretization by means of a finite element method. Next, the different ingredients present in our numerical formulation are detailed and two numerical examples are solved. The first example studies the relaxation of membranes starting with different initial configurations and comparing various options available in our implementation. In the second example, we consider a more challenging problem, in which the membranes are subjected to different forcing terms to study the dynamical response. Finally, some conclusions are drawn.

## 2 MATHEMATICAL FORMULATION

We consider the flow over a surface $\Gamma \subset \mathbb{R}^3$ governed by the elastic or bending Canham-Helfrich energy (Canham (1970))

$$\mathcal{E}(\Gamma) = \frac{C_H}{2} \int_\Gamma \kappa^2, \tag{1}$$

where $\kappa$ stands for the mean curvature of $\Gamma$ and $C_H$ is a material dependent parameter. The rheology of the interface $\Gamma$ is governed by the Boussinesq-Scriven law. According to this, the stresses on the surface can be expressed as

$$\boldsymbol{\sigma}^{(\Gamma)} = \lambda_s \, \mathbf{P} \, \nabla_\Gamma \cdot \mathbf{u} + 2 \, \mu_s \, D_\Gamma \mathbf{u} \tag{2}$$

where $\lambda_s$ and $\mu_s$ are surface viscosity coefficients, $\mathbf{P}$ is the tangent projector onto $\Gamma$ given by

$$\mathbf{P} = \mathbf{I} - \check{\mathbf{n}} \otimes \check{\mathbf{n}}, \tag{3}$$

$\check{\mathbf{n}}$ the normal to $\Gamma$, $\nabla_\Gamma$ the surface gradient operator ($= \mathbf{P}\nabla$) and $D_\Gamma$ is defined as

$$D_\Gamma \mathbf{u} = \frac{1}{2} \, \mathbf{P} \, (\nabla_\Gamma \mathbf{u} + \nabla_\Gamma^T \mathbf{u}) \, \mathbf{P} \tag{4}$$

### 2.1 Variational formulation

According to the virtual work principle, the virtual viscous dissipation over the membrane must balance the virtual work done by all forces present, i.e.,

$$\mathscr{D}_\Gamma(\mathbf{u}, \mathbf{v}) = \int_\Gamma \boldsymbol{\sigma}^{(s)} : (\mathbf{P} \, \nabla_\Gamma \mathbf{v}) = \int_\Gamma [\lambda_s \, \mathbf{P} \, \nabla_\Gamma \cdot \mathbf{u} + 2 \, \mu_s \, D_\Gamma \mathbf{u}] : (\mathbf{P} \, \nabla_\Gamma \mathbf{v}) = \int_\Gamma \mathbf{f}_H \cdot \mathbf{v} \tag{5}$$

The force term $\mathbf{f}_H$ in the right hand side of (5) is taken as $f \, \check{\mathbf{n}}$ with $f$ being the solution of the following variational problem

$$\int_\Gamma f \, \phi = -d\mathcal{E}(\Gamma, \phi) = -C_H \int_\Gamma (\nabla_\Gamma \kappa \cdot \nabla_\Gamma \phi - \frac{\kappa^3}{2} \phi) \tag{6}$$

where $d\mathcal{E}(\Gamma, \phi)$ is the shape derivate of $\mathcal{E}(\Gamma)$ in the direction of the virtual field $\phi$.

**Remark:** The forcing term used in equation (5) is certainly not the only possibility. The shape derivative of $\mathcal{E}(\Gamma)$ with respect to the virtual displacement field $\mathbf{v}$ can be computed instead, and therefore leading to a different formulation. This is proposed in Bonito et al. (2010) and is also the subject of ongoing work.

### 2.2 Area and volume restrictions

As previously mentioned, the membrane is subjected to area and volume restrictions. These constraints are expressed by

$$A(\Gamma(t)) = \mathcal{A}(t), \quad V(\Gamma(t)) = \mathcal{V}(t) \;\; \forall\, t. \tag{7}$$

where the area $A$ and volume $V$ are computed at each time according to

$$A(\Gamma(t)) = \int_{\Gamma(t)} 1 \, d\Gamma, \qquad V(\Gamma(t)) = \int_{\Gamma(t)} \frac{1}{3}\, \mathbf{X} \cdot \hat{\mathbf{n}} \, d\Gamma \tag{8}$$

with $\mathbf{X} : \Gamma \to \mathbb{R}^3$ is the identity function over $\Gamma$. $\mathcal{A}(t)$ and $\mathcal{V}(t)$ are known functions, which in general are taken to be constants equal to the initial area $A(t=0)$ and volume $V(t=0)$ of $\Gamma$ respectively. The area constraint means that the velocity $\mathbf{u}$ must be surface divergence free ($\nabla_\Gamma \cdot \mathbf{u}$). As said before, this work deals in two different ways with this constraint. The first one consists simply in increasing the surface viscosity coefficient $\lambda_s$ with respect to the other coefficient $\mu_s$ in ( 2). Heuristically, this is justified based on the following observation. First, notice that the viscous dissipation can be written as

$$\mathscr{D}_\Gamma(\mathbf{u}, \mathbf{v}) = \int_\Gamma \left[ (\lambda_s \, \nabla_\Gamma \cdot \mathbf{u}) \, (\nabla_\Gamma \cdot \mathbf{v}) + 2 \, \mu_s \, D_\Gamma \mathbf{u} : (\mathbf{P} \, \nabla_\Gamma \mathbf{v}) \right] \tag{9}$$

In the limit with $\lambda_s \to \infty$ we see that $\lambda_s \, \nabla_\Gamma \cdot \mathbf{u}$ will act penalizing the term $\nabla_\Gamma \cdot \mathbf{v}$, without actually adding the restriction to the system. This formulation is specially appealing for level set type formulations. A potential drawback of this approach is the very well known phenomenon of locking, which is indeed not observed in the numerical experiments reported below. Results are however not as promising when the alternative formulation proposed in Bonito et al. (2010) is used instead. In our Lagrangian formulation, the other possible approach that can be adopted without major difficulty consists in effectively adding a surface pressure $\pi_s$ acting as a local Lagrange multiplier. The pressure $\pi_s$ can also be seen as a variable surface tension coefficient. This approach would be cumbersome in a formulation with implicit representation of the interface.

The volume restriction is imposed globally by adding a single internal pressure that acts as a Lagrange multiplier. Alternative ways at dealing with these restrictions can be found in Bonito et al. (2010); Barrett et al. (2008).

The complete continuous variational formulation can then be written as
*"Find* $(\mathbf{u}, \pi_s, p_0) \in V \times Q \times \mathbb{R}$ *such that*

$$\mathscr{D}_\Gamma(\mathbf{u}, \mathbf{v}) - \int_\Gamma \pi_s \, \nabla_\Gamma \cdot \mathbf{v} - p_0 \int_\Gamma \mathbf{v} \cdot \check{\mathbf{n}} \;=\; \int_\Gamma \mathbf{f}_H \cdot \mathbf{v} \tag{10}$$

$$r \int_\Gamma \mathbf{u} \cdot \check{\mathbf{n}} \;=\; 0 \tag{11}$$

$$\int_\Gamma q \, \nabla_\Gamma \cdot \mathbf{u} \;=\; 0 \tag{12}$$

*for all* $(\mathbf{v}, q, r) \in V \times Q \times \mathbb{R}$*"*, where $V$ and $Q$ are suitable function spaces for the velocity $\mathbf{v}$ and the surface pressure $\pi_s$.

## 3 DISCRETE FORMULATION

The resolution of the problem above is difficult in general, because of the non–linearities and the need for an accurate estimate for $\kappa$ appearing in the forcing term (6).

In this work, two methods are considered to compute the curvature. The first one is a geometrical method proposed by Meyer. For the sake of brevity we refer the reader to Meyer et al. (2002) for details. The other method tested is based on the Laplace-Beltami identity, which, for a closed surface $\Gamma$ reads

$$\int_\Gamma \boldsymbol{\mathcal{K}} \cdot \mathbf{v}\, d\Gamma = \int_\Gamma \Delta_\Gamma \mathbf{X} \cdot \mathbf{v}\, d\Gamma = -\int_\Gamma \nabla_\Gamma \mathbf{X} : \nabla_\Gamma \mathbf{v}\, d\Gamma \tag{13}$$

then, the mean curvature $\kappa$ is equal to $\| \boldsymbol{\mathcal{K}} \|$.

The complete numerical formulation proposed is described now. We begin with an initial representation of $\Gamma$ at $t = 0$, which is a finite element partition $\mathcal{T}_h$ made of linear (planar) or quadratic (curved) isoparametric triangular elements. For any point $\mathbf{X}$ on a given element we can write

$$\mathbf{X}(\xi_1, \xi_2, \xi_3) = \sum_J^{N_p} \mathbf{X}_J\, N_J(\xi_1, \xi_2) + \check{\mathbf{n}}_h\, \xi_3 \tag{14}$$

where $\mathbf{X}_J$ is the coordinate position of node $J$, $N_J$ is the nodal basis function of node $J$ and $(\xi_1, \xi_2, \xi_3)$ are coordinates in a reference element. With the normal extension used in (14), the isoparametric map between a triangle in $\mathbb{R}^3$ and a reference one in $\mathbb{R}^2$ becomes straightforward.

As already mentioned, a stabilization by pressure gradient projection is used to avoid spurious pressure modes (see Codina et al. (2001)). A estabilization is also needed in the computation of the Willmore force and the curvature by means of the Laplace-Beltrami approach. The discrete variational formulation is very much based on that one for the standard Stokes problem, but replacing the viscous operator by the Boussinesq-Scriven law and using the surface nabla operator $\nabla_\Gamma$ to compute derivatives over $\Gamma$. The formulation is divided in the following steps 1 to 5:

### Step 1: Curvature computation

If the Laplace-Beltrami approach is used, the discrete mean curvature is given as

$$\kappa_h = (\kappa_{1h}^2 + \kappa_{2h}^2 + \kappa_{3h}^2)^{\frac{1}{2}} \tag{15}$$

where $\kappa_{ih},\ (i = 1, 2, 3)$ is the solution of the following problem

*"Find* $\kappa_{ih}^n \in W_h$ *such that*

$$\int_\Gamma \kappa_{ih}\, \phi_h + \sum_{K \in \mathcal{T}_h} \int_K \tau \nabla_\Gamma \kappa_{ih} \cdot \nabla_\Gamma \phi_h = -\int_\Gamma \nabla_\Gamma \mathbf{X}_{ih} \cdot \nabla_\Gamma \phi_h \tag{16}$$

*for all* $\phi_h \in W_h$*"*. The space $W_h$ is made up of linear or quadratic continuous functions. The parameter $\tau$ is made equal to $h^2/4$ for linears and $h^2/16$ for quadratics, with $h$ the local element size. Otherwise, if the geometrical Meyer's method is used to compute the curvature instead, this first step is not performed.

**Step 2: Bending force computation**

Once the curvature is known, the bending force can be computed as solution of the next variational problem

*"Find* $f_h \in W_h$ *such that*

$$\int_{\Gamma_h^n} f_h^n \, \phi_h + \sum_{K \in \mathcal{T}_h} \int_K \tau \nabla_\Gamma f_h \cdot \nabla_\Gamma \phi_h = -C_H \int_{\Gamma_h^n} (\nabla_\Gamma \kappa_h^n \cdot \nabla_\Gamma \phi_h - \frac{\kappa_h^{n3}}{2} \phi_h) \tag{17}$$

*for all* $\phi \in W_h$*"*

**Step 3: Pressure gradient projection**

The pressure gradient projection is taken at time $n$, assuming it equal to zero at the beginning of the simulation for simplicity. The projection is obtained as solution of

*"Find* $\boldsymbol{\xi}_h^n \in S_h$ *such that*

$$\int_{\Gamma_h^n} \boldsymbol{\xi}_h^n \cdot \boldsymbol{\eta} = \int_{\Gamma_h^n} \nabla_\Gamma {\pi_s}_h^n \cdot \boldsymbol{\eta} \tag{18}$$

*for all* $\boldsymbol{\eta} \in \times S_h$*"*, where the space $S_h$ is made up of linear continuous functions.

**Step 4: Velocity-Pressure computation**

Finally, the new velocity field can be computed by solving the viscous operator over the surface as follows

*"Find* $(\mathbf{u}_h^{n+1}, {\pi_s}_h^{n+1}, p_0^{n+1}) \in V_h \times Q_h \times \mathbb{R}$ *such that*

$$\mathscr{D}_\Gamma(\mathbf{u}_h^{n+1}, \mathbf{v}_h) - \int_{\Gamma_h^n} \beta \, \mathbf{u}_h^{n+1} \cdot \mathbf{v}_h + \int_{\Gamma_h^n} {\pi_s}_h^{n+1} \nabla_\Gamma \cdot \mathbf{v} - p_0^{n+1} \int_{\Gamma_h^n} \mathbf{v}_h \cdot \check{\mathbf{n}}_h = \int_{\Gamma_h^n} f_h^n \, \check{\mathbf{n}}_h \cdot \mathbf{v}_h \tag{19}$$

$$r \int_{\Gamma_h^n} \mathbf{u}_h^{n+1} \cdot \check{\mathbf{n}}_h = 0 \tag{20}$$

$$\int_{\Gamma_h^n} q_h \, \nabla_\Gamma \cdot \mathbf{u}_h^{n+1} + \sum_{K \in \mathcal{T}_h} \int_K \tilde{\tau} \nabla_\Gamma q_h \cdot (\nabla_\Gamma {\pi_s}_h^{n+1} - \boldsymbol{\xi}^n) = 0 \tag{21}$$

*for all* $(\mathbf{v}, q, r) \in V_h \times Q_h \times \mathbb{R}$*"*, where the parameter $\tilde{\tau} = h^2/4\mu_s$. Noticed that a dissipation proportional to the velocity has also been added to (19), which helps to avoid infinite dissipation modes. The velocity space $V_h$ is made up of linear or quadratic continuous functions and the space $Q_h$ of linear continuous functions. When quadratic elements are used for $V_h$ (and also for $W_h$) the estabilization coefficient $\tilde{\tau}$ is made equal to zero and the pressure gradient projection step simply ignored.

**Step 5: Lagrangian update**

Once the velocity field has been computed, the new surface $\Gamma_h^{n+1}$ is found by simple update of the nodal positions as

$$\mathbf{X}_h^{n+1} = \mathbf{X}_h^n + \Delta t\, \mathbf{u}_h^{n+1} \tag{22}$$

Finally, at each time, $\Delta t$ is adjusted to $0.1\, h_{\min}/\| \mathbf{u}_h \|_{\max}$, so as to avoid large distorsions and possible inversions of the mesh triangles.

## 4 NUMERICAL RESULTS

### 4.1 Relaxation to oblate and prolate shapes

We first study the relaxation of biological membranes starting from ellipsoidal shapes. The material parameters used for the simulations are $\mu_s = 1$, $\lambda_s = 2$, $C_H = 10^{-3}$. Quadratic elements are used for interpolation of geometry and velocity field and linear elements for membrane pressure. The parameter $\beta$ was made equal to 1 in all the simulations. We present results for two differents initial shapes. Figure 1 shows the shape of the membrane at different instants corresponding to a $0.15 \times 1 \times 1$ initial ellipsoid towards an oblate shape typical of discocytes and is actually in good qualitative agreement with the shapes observed in red blood cells. Figure 2 similarly shows the evolution of a $0.25 \times 0.25 \times 1$ initial ellipsoid towards a prolate shape.

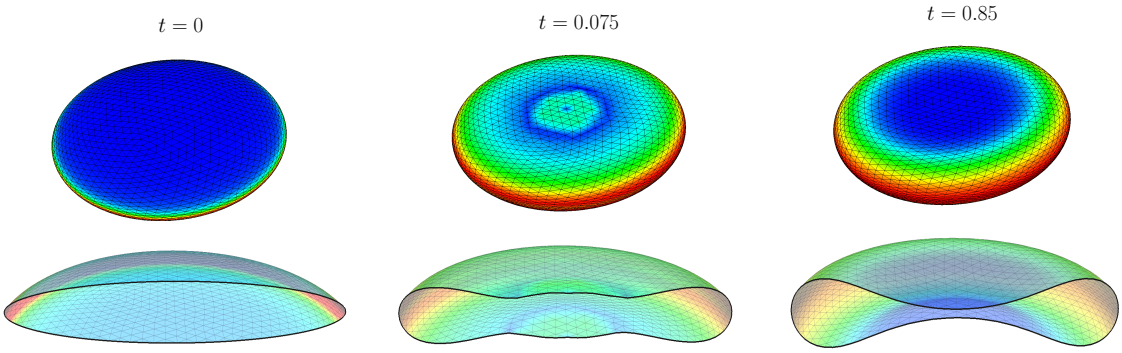


Figure 1: Relaxation of a $0.15 \times 1 \times 1$ initial ellipsoid to an oblate shape typical of discocytes. The membrane is painted with the mean curvature.

In these problems, it is interesting to observe the evolution of the Canham-Helfrich energy as a function of time. In figure 3 we show the non-dimensional energy for each case. We see that, after the sudden change at the beginning, the membrane ends up relaxing towards an energy minimum. This minimum value depends on the reduced volume of the membrane and can logically be affected by discretization errors. In figure 4 we plot the area as a function of time for different values of $\lambda_s$ (and ignoring the pressure $\pi_s$ in the computation) and solving with the membrane pressure (with $\lambda_s = 0$). In all cases, area is well preserved as noticed in the figures. In fact, most of the area lost come from the explicit Lagrangian update, as it can be verified by refining the time step. Finally, to see the effect of different discretization issues, we show in figure 5 the energy as a function of time for the relaxation of an initial $0.2 \times 0.2 \times 1$ ellipsoid in the following cases:

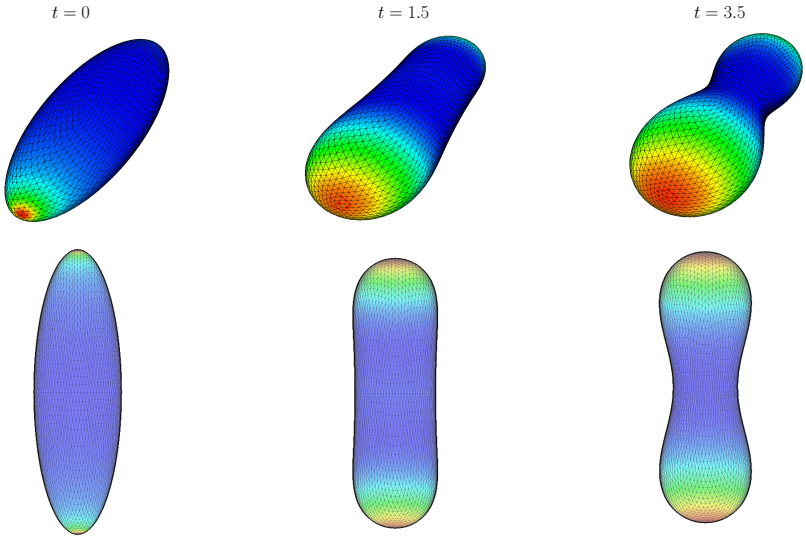


Figure 2: Relaxation of a $0.25 \times 0.25 \times 1$ initial ellipsoid to a prolate shape. The membrane is painted with the mean curvature.

(i) coarse mesh with linear elements and Laplace-Beltrami method;

(ii) coarse mesh with linear elements and Meyer's method;

(iii) coarse mesh with quadratic elements and Laplace-Beltrami;

(iv) fine mesh with linear elements and Laplace-Beltrami;

the coarse mesh having 1280 elements and the fine one 5120. We clearly see a significant difference of case (i) with respect to the other simulated cases. Cases (iii) and (iv) give very similar results with similar computational costs.

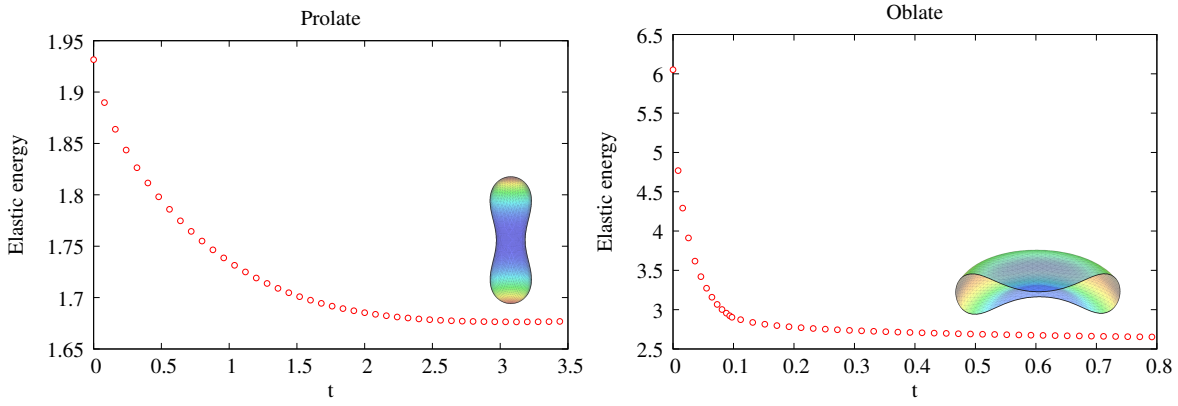


Figure 3: Energy as a function of time for the relaxation of membranes towards the prolate and oblate shapes.

## 4.2 Forced discocyte

We simulate now a more challenging problem to test the robustness of the methodology. In this case we consider a $0.2 \times 1 \times 1$ initial ellipsoid over which an oscillatory force is applied.

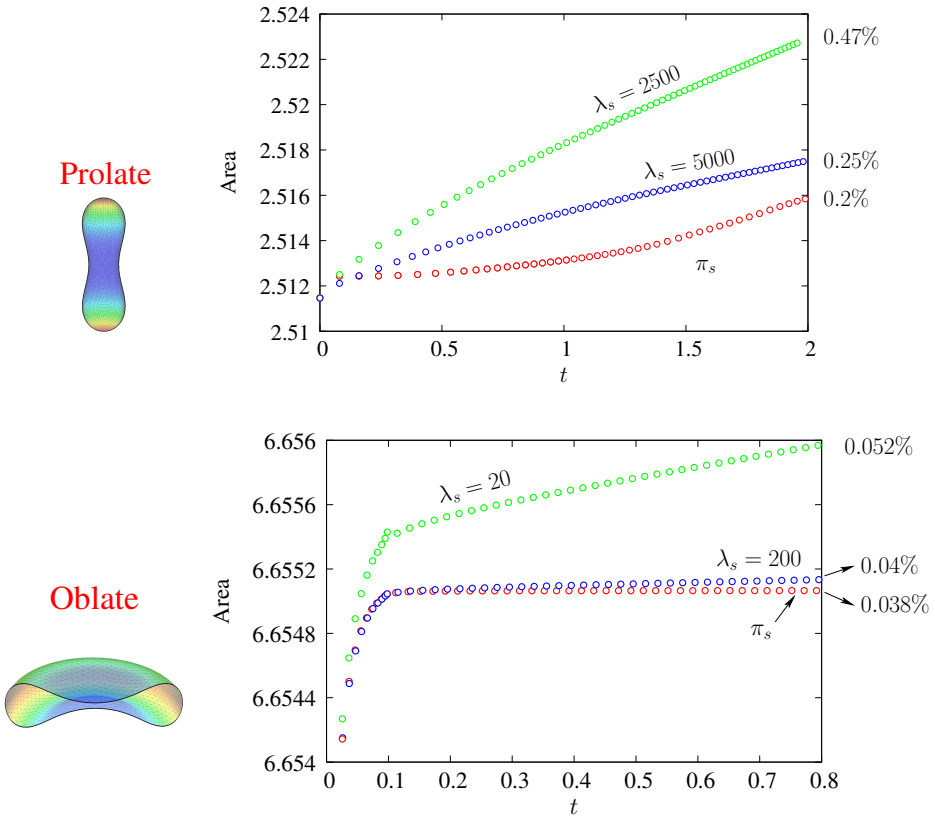


Figure 4: Area as a function of time for the relaxation of membranes towards the prolate and oblate shapes for different values of $\lambda_s$.

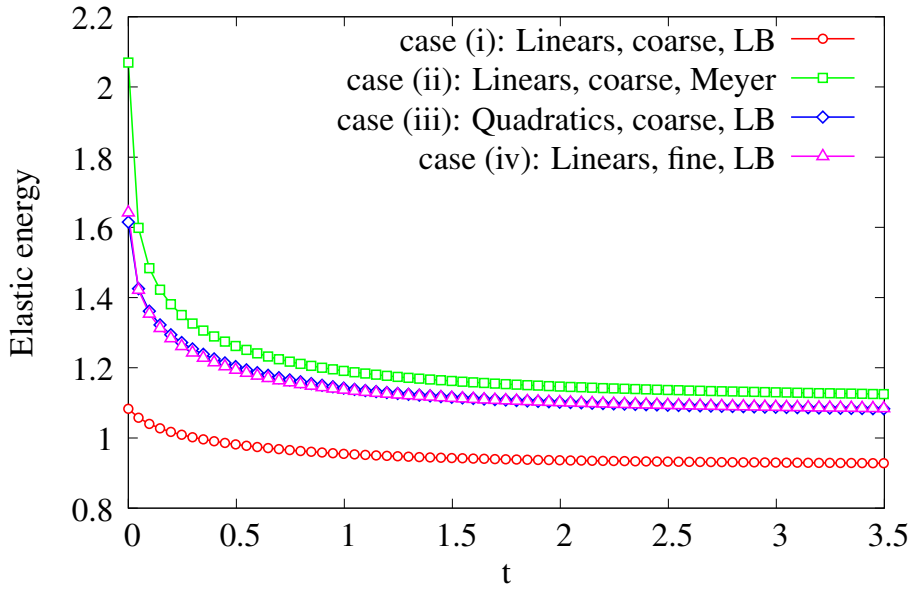


Figure 5: Energy as a function of time for the relaxation of a membrane towards the oblate shape comparing the different options (i)-(iv).

This force depends on the sign of an indicator function $\phi$ which ranges from $-1$ to 1 as shown in the first detail of figure 6 and is given by

$$g(\mathbf{x}) = \begin{cases} +\frac{1}{4}\cos(\pi t)\,\check{\mathbf{n}} & \text{if } \phi(\mathbf{x}) \geq 0 \\ -\frac{1}{4}\cos(\pi t)\,\check{\mathbf{n}} & \text{if } \phi(\mathbf{x}) < 0 \end{cases} \tag{23}$$

The force is added to the right hand side of (19). For this simulation a mesh consisting of 5120 linear triangles is used together with Meyer's method to compute the curvature. The material parameters are: $\mu_s = 1$, $\lambda_s = 2$, $C_H = 10^{-3}$ and $\beta = 1$. As seen in figure 6, after an initial transient the energy exhibits an oscillatory behavior with the same period of the applied force. At different instants, a detail coloured with the membrane pressure shows the shape of the discocyte.

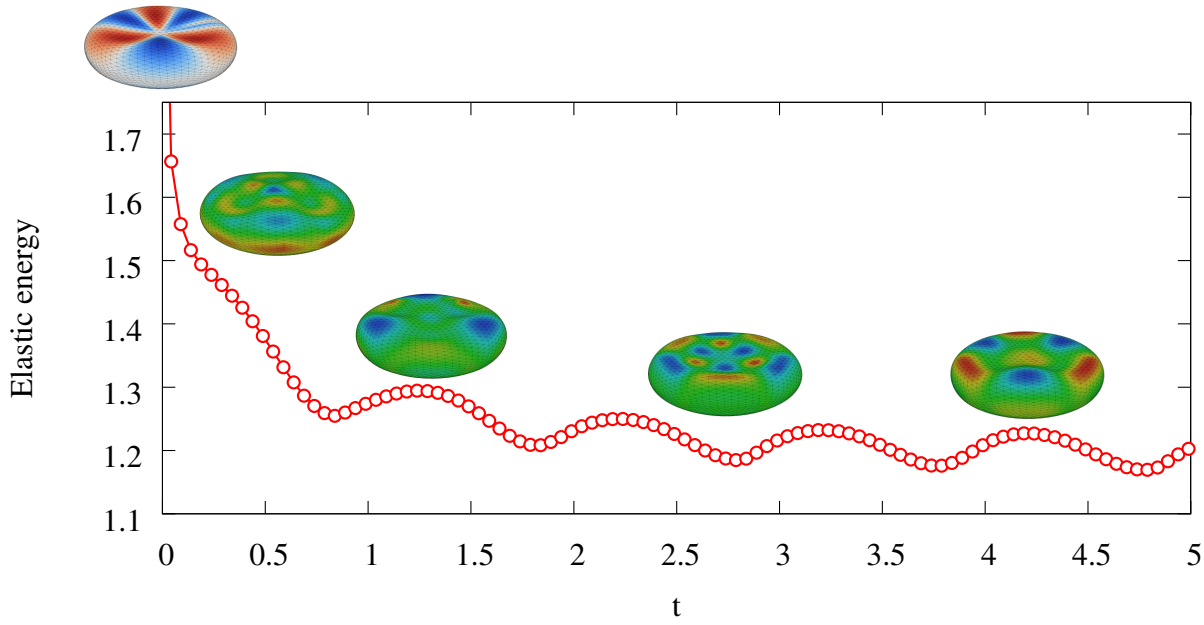


Figure 6: Energy as a function of time for the forced discocyte. The first detail at $t = 0$ shows the indicator function used to apply the force given by (23). The same pattern is present on the bottom part of the membrane. The color scale goes from $-1$ (blue) to 1 (red). For the shapes at times $t = 0.46,\ 1.3,\ 2.8,\ 4.1$ the color scale corresponds to membrane pressure.

## 5 CONCLUSIONS

A Lagrangian finite element formulation for the simulation of viscous membranes governed by the Boussinesq-Scriven law and the Canham-Helfrich energy with surface area and volume restrictions has been presented. The area constraint was included in the formulation by means of increasing one surface viscosity coefficient or by means of a local Lagrange multiplier. The volume constraint was included by means of adding an internal pressure. Two problems have been solved with this formulation. The first problem studied the relaxation of membranes and was meant to test the various ingredients present in the formulation. It was found that using linear elements on a fine grid produces similar results as compared to quadratic ones on a coarser grid. The area was well preserved by means of the two approaches considered. The second problem studied the evolution of a discocyte subjected to an oscillatory force to test robustness

of the formulation. Further work include a thorough quantitave comparison of results with theoretical and/or experimental ones and implementation of adaptive mesh refinement to solve problems such as membrane tethering, which involves larger deformations of the membranes.

## ACKNOWLEDGMENTS

The authors acknowledge partial support from FAPESP (Brazil), CNPq (Brazil), This research was carried out in the framework of INCT-MACC, Ministério de Ciência e Tecnologia, Brazil.

## REFERENCES

Arroyo M. and DeSimone A. Relaxation dynamics of fluid membranes. *Phys. Rev. E Stat. Nonlin. Soft Matter Phys.*, 123:031915, 2009.

Bänsch E., Morin P., and Nochetto R.H. A finite element method for surface diffusion: the parametric case. *Journal of Computational Physics*, 203:321–343, 2005.

Barrett J., Garcke H., and Nürnberg R. On the parametric finite element approximation of evolving hypersurfaces in $R^3$. *Journal of Computational Physics*, 227:4281–4307, 2008.

Bonito A., Nochetto R., and Pauletti S. Dynamics of biomembranes: Effect of the bulk fluid. *Math. Model. Nat. Phenom.*, 6(22):25–43, 2011.

Bonito A., Nochetto R.H., and Pauletti M.S. Parametric FEM for geometric biomembranes. *Journal of Computational Physics*, 229(9):3171–3188, 2010.

Bothe D. and Prüss J. On the Two-Phase Navier-Stokes Equations with Boussinesq-Scriven Surface Fluid. *Journal of Mathematical Fluid Mechanics*, 12(1):133–150, 2010.

Buscaglia G. and Tasso I. A finite element method for viscous membranes. *Submitted to Computational Methods in Applied Mechanics and Engineering*, 2011.

Canham P. The minimum energy of bending as a possible explanation of the biconcave shape of the human red blood cell. *Journal of Theoretical Biology*, 26:61–81, 1970.

Codina R., Blasco J., Buscaglia G.C., and Huerta A. Implementation of a stabilized finite element formulation for the incompressible Navier-Stokes equations based on a pressure gradient projection. *International Journal for Numerical Methods in Fluids*, 37(4):419–444, 2001.

Gross S. and Reusken A. *Numerical Methods for Two-phase Incompressible Flows,*. Springer Series in Computational Mathematics, Vol. 40, 2011.

Meyer M., Desbrun M., Schröder P., and Barr A. Discrete differential geometry operators for triangulated 2-manifolds. *Proc. VisMath'02, Berlin*, 2002.

Pozrikidis C. Effects of surface viscosity on the finite deformation of a liquid drop and the rheology of dilute emulsions in simple shearing flow. *Journal of Non-Newtonian Fluid Mechanics*, 1(93):161–178, 1994.

Salac D. and Miksis M. A level set projection model of lipid vesicles in general flows. *Journal of Computational Physics*, 230(22):8192–8215, 2011.

Seifert U. Fluid membranes in hydrodynamic flow fields: Formalism and an application to fluctuating quasi-spherical vesicles in shear flow. *The European Physical Journal B - Condensed Matter and Complex Systems*, 8:405–415, 1999.

Waugh R. Surface viscosity measurements from large bilayer vesicle tether formation. *Biophysics Journal*, 38:29–37, 1982.